Journal of Power Sources 195 (2010) 2877–2882

Contents lists available at ScienceDirect

Journal of Power Sources

journal homepage: www.elsevier.com/locate/jpowsour

Hydrothermal preparation of $LiFePO_4$ nanocrystals mediated by organic acid

Jiangfeng Ni[a,*], Masanori Morishita[b], Yoshiteru Kawabe[b], Masaharu Watada[b], Nobuhiko Takeichi[a], Tetsuo Sakai[a,*]

[a] National Institute of Advanced Industrial Science and Technology, Kansai Center, 1-8-31 Midorigaoka, Ikeda, Osaka 563-8577, Japan
[b] GS Yuasa Corporation, Nishinosho, Kisshoin, Minami-ku, Kyoto 601-8520, Japan

ARTICLE INFO

Article history:
Received 21 July 2009
Received in revised form 2 November 2009
Accepted 2 November 2009
Available online 10 November 2009

Keywords:
Lithium ion battery
Cathode
$LiFePO_4$
Hydrothermal
Nanocrystal
Synchrotron radiation

ABSTRACT

Well-crystallized $LiFePO_4$ nanoparticles have been directly synthesized in a short time via hydrothermal process in the presence of organic acid, e.g. citric acid or ascorbic acid. These acid-mediated $LiFePO_4$ products exhibit a phase-pure and nanocrystal nature with size about 50–100 nm. Two critical roles that the organic acid mediator plays in hydrothermal process are recognized and a rational mechanism is explored. After a post carbon-coating treatment at 600 °C for 1 h, these mediated $LiFePO_4$ materials show a high electrochemical activity in terms of reversible capacity, cycling stability and rate capability. Particularly, $LiFePO_4$ mediated by ascorbic acid can deliver a capacity of 162 mAh g^{-1} at 0.1 C, 154 mAh g^{-1} at 1 C, and 122 mAh g^{-1} at 5 C. The crystalline structure, particle morphology, and surface microstructure were characterized by high-energy synchrotron X-ray diffraction (XRD), transmission electron microscopy (TEM) and scanning electron microscopy (SEM), and Raman spectroscopy, respectively. And the electrochemical properties were thoroughly investigated by galvanostatic test and electrochemical impedance spectroscopy (EIS).

© 2009 Elsevier B.V. All rights reserved.

1. Introduction

Olivine $LiFePO_4$ has been regarded as one of the most promising cathode materials for advanced Li ion battery for use in high energy and power system as required for plug-in hybrid electric vehicles (PHEV) [1–3]. Although it displays plenty of attractive characters such as good electrochemical property, high thermal stability, and environmental benignity, the low electronic/ionic conductivity makes it not a competent candidate for use in high power devices.

Over the last decade, enormous attempts have been made to improve its conductivity to applicable level. A successful strategy is the preparation of $LiFePO_4$–carbon composite [4–7], where $LiFePO_4$ particles are incorporated into carbon network, bringing the total conductivity to a level similar to $LiCoO_2$. This $LiFePO_4$/C composite is generally synthesized by an in situ carbon-coating route during which the carbon decomposed from organic precursor deposits on the $LiFePO_4$ surface to form a high way for electron movement. An additional benefit arisen from this process is the inhibiting of particle fusion and growth by exotic carbon layer, which helps achieve high rate ability. Doping of divalent (Mg^{2+}, Mn^{2+}, Ni^{2+}, Cu^{2+}) or supervalent ions (Al^{3+}, Cr^{3+}, Zr^{4+}, Nb^{5+}) either in Li site (M1) or in Fe site (M2) has also been demonstrated to improve the electronic conductivity successfully [7–9], but so far the mechanism is still in great controversial [10,11]. Recently, the application of cutting-edge nanotechnology in the synthesis of $LiFePO_4$ has been demonstrated, too. With template, $LiFePO_4$ of particular morphology such as nanofibre or nanowire has been prepared, and it demonstrates potential for high power application [12,13].

Although the conductivity problem are solved to a large extent by methods mentioned above, application of $LiFePO_4$ still suffers from tough synthesis procedure resulting from instable nature of Fe(II). The popular strategy to synthesize $LiFePO_4$ is the high-temperature ceramic route under the inert atmosphere, which results in a final product frequently composed of impurities like $Li_3Fe_2(PO_4)_3$, Fe_2O_3, and Li_3PO_4 [14,15]. And it is also very difficult by such process to obtain fine and homogeneous particle that is regarded as a key factor for the power ability [16].

To obtain $LiFePO_4$ with fine particles for high power purpose, it is essential to take advantage of solution synthetic route such as precipitation [16], sol–gel [17], polyol [18], and hydrothermal [19–25]. Among them, hydrothermal reaction receives particular interest due to mild operating temperature, simple process, high crystallization of product, and the potential for large-scale production. It is also considerably convenient to control the properties of product by tuning experiment parameters such as temperature, pressure, concentration, and additive. In a pioneering attempt, Whittingham and co-workers displayed the synthesis of $LiFePO_4$ via hydrothermal reaction at 120 °C, but the product showed a low electrochemical

* Corresponding authors. Tel.: +81 72 751 9611; fax: +81 72 751 9623.
E-mail addresses: jfengni@gmail.com, jiangfeng.ni@aist.go.jp (J. Ni), sakai-tetsuo@aist.go.jp (T. Sakai).

0378-7753/$ – see front matter © 2009 Elsevier B.V. All rights reserved.
doi:10.1016/j.jpowsour.2009.11.017

activity due to a severe displacement of Fe in Li site [19]. A following report by them demonstrated that the displacement of Fe and Li could be remarkably suppressed when arising temperature above 180 °C [20]. However, many displacement-free materials do not show satisfactory electrochemical behavior, probably due to grown particle size [20,21] or the presence of impurities [22,23]. Recently, Nazar and co-workers reported that $LiFePO_4$ nanocrystallites could be obtained under hydrothermal condition by increasing reagents concentration or adding organic additives like polyacrylic acid and ascorbic acid, but not citric acid [24]. However, their material does not show favorable electrochemical performance as expected, possibly due to grain agglomeration. Special strategy involving the application of surfactants has been demonstrated to effectively control the crystalline property and particles size of $LiFePO_4$, leading to a pronounced improved performance. A good case in point is the synthesis of C/$LiFePO_4$ core/shell nanomaterial via hydrothermal route using acetylene black as nucleus and dioxane as surfactant in the presence of polyethylene glycol [25]. The resultant material shows an excellent rate ability, but the high carbon content (52 wt.%) makes it not suitable for practical application.

So far, it is still a significant challenge to prepare high-performance $LiFePO_4$ by a simple hydrothermal reaction. And the role that the organic additive plays in the crystalline and electrochemical properties has not been well appreciated. Herein we report the synthesis of phase-pure $LiFePO_4$ nanocrystal by a facile hydrothermal process mediated by organic acid, i.e. citric acid or ascorbic acid. The crystalline nature, particle property, and surface depending on additive have been investigated by high-energy synchrotron X-ray diffraction (XRD), scanning electron microscopy (SEM), transmission electron microscopy (TEM), and Raman spectroscopy. The electrochemical properties were thoroughly researched by galvanostatic test and electrochemical impedance spectroscopy (EIS).

2. Experimental

$LiFePO_4$ was prepared via the hydrothermal route from starting materials $FeSO_4{\cdot}7H_2O$, H_3PO_4, and $LiOH{\cdot}H_2O$ in a molar ratio of 1:1:3. First, 0.03 mol LiOH aqueous solution was mixed with 0.01 mol H_3PO_4 at vigorous agitation to form white suspension of Li_3PO_4. And then a mixing solution of 0.01 mol $FeSO_4{\cdot}7H_2O$ and 1.67 mmol organic acid additive, i.e., citric acid or ascorbic acid, was added to the suspension dropwise, which resulted in a pH value ~4.6. The final products were labeled according to the additive quoted as F-citric and F-ascorbic. After stirring for 5 min followed by Ar-gas bubbling for 10 min, this suspension (~40 mL) was transferred into an stainless steel autoclave (Taiatsu Japan, inside volume 300 ml), and then reacted at 230 °C for 30 min. It should be noted the internal atmosphere of the autoclave was exchanged by Ar gas prior to heating, and that the time for the temperature rising to 230 °C is about 30 min. After reaction, the resultant light-green precipitation was collected, washed by water and ethanol for several times, and dried at 80 °C in vacuum. To improve the conductivity, the obtained material was further mixed with citric acid and treated at 600 °C for 1 h under Ar atmosphere. The final product contains about 2 wt.% carbon, as determined by TG analysis. For comparison, the blank $LiFePO_4$ (labeled as F-blank) was also prepared by the same procedure but no additive added over the hydrothermal step.

The XRD measurements were conducted using a large Debye–Scherrer camera with an imaging plate at the BL19B2 beam line, the synchrotron radiation facility SPring-8, Japan. A glass capillary of φ 0.3 mm was used as the holder for filling the sample powder. The diffraction patterns were recorded in the 2θ range of 0.01–78° with duration of 5 min. The wavelength λ = 0.7006 Å was calibrated by using CeO_2 as standard material. The structural analyses were performed with the Rietveld method on the program Rietan-2000 [26].

SEM and TEM were performed to observe the particle morphology and size distribution. SEM images were taken on a JEOL JSM-6390 microscope at an accelerating voltage of 30 kV. TEM was performed on a JEOL JEM-3000F transmission electron microscope at an accelerating voltage of 300 kV. Raman spectroscopy was carried out to study the surface microstructure, using a RMP-320 (Jasco) spectrometer with Ar laser of 50 mW at 532 cm^{-1}.

For the electrochemical test, 80 wt.% as-prepared $LiFePO_4$ material, 10 wt.% ketjen black, and 10 wt.% polyvinylidene were blended in N-methylpyrrolidinon. The blended slurry was then casted on an aluminum foil followed by roll processing. Afterward, the electrode sheet was tailored to disks shape of φ 12 mm with a typical material loading of 5 mg cm^{-2} and dried at 120 °C for 6 h in vacuum. A 2032 coin cell was assembled using the disk electrode as cathode in a dry room with a dewpoint below −60 °C. The anode is Li foil and the electrolyte is 1 mol L^{-1} $LiPF_6$ in ethylene carbonate/diethyl carbonate (EC/DEC) (1:1, v/v). The cells were tested on a Keisoku Genki program-controlled test system in the voltage range of 2.3–4.2 V at 28 °C.

EIS was carried out with a Solartron SI 1280B electrochemical unit. The applied frequency range is 65 kHz to 0.01 Hz and the oscillation voltage is 10 mV.

3. Results and discussion

3.1. High-energy synchrotron XRD

Fig. 1 shows the XRD patterns of as-prepared three $LiFePO_4$ samples (F-blank, F-citric, and F-ascorbic). All the patterns show well-resolved diffraction peaks indexed to olivine $LiFePO_4$ (JCPDS No. 81-1173). This indicates that well-crystallized $LiFePO_4$ can be readily obtained via hydrothermal reaction at 230 °C in half hour. By contrast, Nazar et al. found that well-crystallized $LiFePO_4$ could be prepared only when hydrothermal reaction extending 5 h at 190 °C [24]. It is also found that the pattern of $LiFePO_4$ prepared without additive shows diffraction peaks at 10.1°, 10.6°, and 11.2° (Fig. 1a), which can be attributed to orthorhombic Li_3PO_4 (JCPDS No. 25-1030), while these peaks were not visible in those of the samples mediated by organic acid (Fig. 1b and c).

The structural refinement has been done for the synchrotron XRD data of as-prepared samples. The R factors and the structural parameters based on the Rietveld refinement of all three samples are summarized in Table 1, and the observed pattern and calculated one of the typical sample F-blank are presented

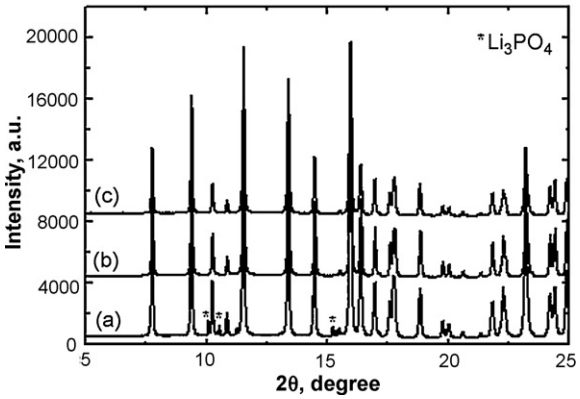

Fig. 1. High energy synchrotron XRD patterns of as-prepared $LiFePO_4$ samples: (a) F-blank, (b) F-citric, and (c) F-ascorbic.

Table 1
The R factors and structural parameters of as-prepared $LiFePO_4$ materials.

Sample	Phase	a (Å)	b (Å)	c (Å)	V (Å^3)	R_{wp} (%)	R_p (%)	S	Content (wt.%)
F-blank	$LiFePO_4$	10.3379(2)	6.0037(1)	4.6977(1)	291.568	5.20	3.79	1.540	97.32
	Li_3PO_4	6.1153(8)	5.2394(6)	4.8683(5)	155.990				2.68
F-citric	$LiFePO_4$	10.3351(1)	6.0052(1)	4.6976(1)	291.556	3.94	3.01	1.164	100
F-ascorbic	$LiFePO_4$	10.3378(1)	6.0027(1)	4.6989(1)	291.588	4.45	3.38	1.096	100

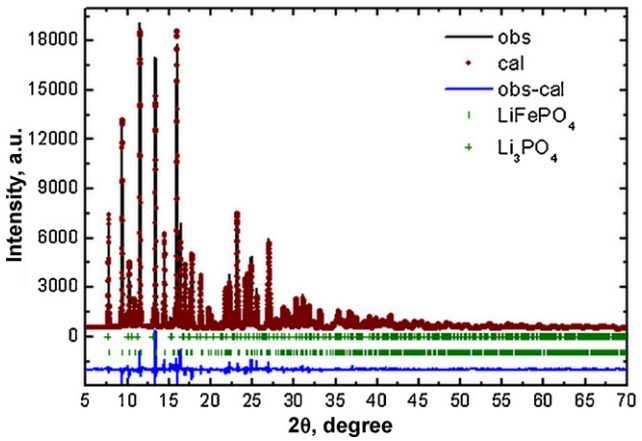

Fig. 2. The observed XRD pattern, calculated one and their difference based on the Rietveld refinement of F-blank sample. The Bragg positions of $LiFePO_4$ and Li_3PO_4 are also shown.

in Fig. 2. The refinement for F-blank is based on $LiFePO_4$–Li_3PO_4 two-phase model and that for the mediated materials is based on $LiFePO_4$ single phase model. All refinements give a small value of factors R_{wp}, R_p, and S, indicative of a good and reliable structural analysis. F-blank is composed of 97.32 wt.% $LiFePO_4$ phase and 2.68 wt.% Li_3PO_4 phase, while the mediated samples show single phase nature. This indicates that the growth of impurities like Li_3PO_4 can be effectively suppressed by organic acids, which may refers to their multiple effects on hydrothermal system such as pH value, solubility, complex ingredient and so forth. The olivine phase in F-blank has the lattice parameters of $a = 10.3379(2)$ Å, $b = 6.0037\,(1)$ Å, $c = 4.6977(1)$ Å, and $V = 291.568$ Å^3, close to the values in references [1,24]. And the unit cell volume just falls in the range of 291.4 ± 0.2 Å^3, consistent with the empirical rule for Fe displacement-free $LiFePO_4$ [20]. Similar parameters are also found in the other $LiFePO_4$ samples.

Table 2 lists the atomic parameters of the typical F-ascorbic sample. In $LiFePO_4$ lattice, Li ions occupy 4a site in one set of octahedra, Fe ions occupy 4c site in another set of octahedra, P ions and half O ions occupy 4c site, and the other half O ions occupy 8d site. It is worthy of noting that our attempt to refine the pattern assuming part Fe ion in Li site failed, indicative of no Fe ion occupying Li site.

When LiOH was added to mixture solution of $(NH_4)_2Fe(SO_4)_2$ and H_3PO_4, the solution gradually changed from acidic to neutral and $Fe_3(PO_4)_2{\cdot}8H_2O$ precipitated, as mentioned in previous report [23]. But in our experiment, the feed order was changed; i.e., the $FeSO_4$ solution was added to system of LiOH and H_3PO_4. The process can be expressed as the formation of Li_3PO_4 (Eq. (1)) followed by one unit Fe^{2+} ion replacing two units Li^+ ions and crystallizing (Eq. (2)).

$$3LiOH + H_3PO_4 \rightarrow Li_3PO_4 + 3H_2O \quad (1)$$

$$Li_3PO_4 + FeSO_4 \rightarrow LiFePO_4 + Li_2SO_4 \quad (2)$$

Since Li ions number is far more than Fe^{2+} ion when reaction II close to the end, and the reaction is also limited by the conversion rate, the full conversion of Li_3PO_4 to $LiFePO_4$ is difficult to reach. When 1.67 mmol organic acid is added, the pure $LiFePO_4$ is obtained as the system changes from near neutral (pH ~ 6.7) to acidic (pH ~ 4.6). As is well known, reaction II generally proceeds by a dissolution–precipitation mechanism, which can be accelerated under acidic environment, because proton facilitates the dissolution process. Moreover, the reaction balance may also be adjusted towards $LiFePO_4$ direction by chelating effect of organic acid. For example, citric acid molecule may capsulate Fe^{2+} ion to form $[C_6H_8O_7Fe^{2+}]$, which further combines with $[Li^+PO_4{}^{3-}]$ to form $[C_6H_8O_7Fe^{2+}\cdots Li^+PO_4{}^{3-}]$ ion pairs through the coulombic attraction and then crystallizes by following condensation. As a result, a single phase $LiFePO_4$ material was prepared. A similar mechanism was also proposed by Zhou et al. [27] when they prepared mesoporous $Li_3Fe_2(PO_4)_3$ using CTAB as a template.

From the above discussion, it can be concluded that the acidic effect influences the reaction rate, and the chelating effect adjusts the balance. It is both of these two effects, not any single one of them, that lead to the pure material. To confirm this, we carried out two additional experiments without organic acid to simulate the two effects, respectively. One case concerns merely the chelating effect which was inspected by using polyvinyl alcohol (PVA). Unfortunately, the corresponding XRD pattern (Fig. 3a) displays even more intense peaks due to Li_3PO_4 than F-blank, probably the conversion being blocked as crystallites are covered by PVA molecule. The other case concerns merely the acidic environment which was deliberately created by controlling the ratio of LiOH against H_3PO_4 to 2.5:1. The pH value is about 4.5, very close to that of the organic

Table 2
The atomic parameters for F-ascorbic sample. Here g is the site occupancy and B is the overall isotropic atomic displacement parameter.

Atom	Site	x	y	z	g	B (Å^2)
Li	4a	0	0	0	1	0.5
Fe	4c	0.2817	0.25	0.9736	1	0.033
P	4c	0.0952	0.25	0.4147	1	0.077
O1	4c	0.1000	0.25	0.7462	1	1.052
O2	4c	0.4498	0.25	0.2065	1	1.297
O3	8d	0.1664	0.0423	0.2812	1	0.525

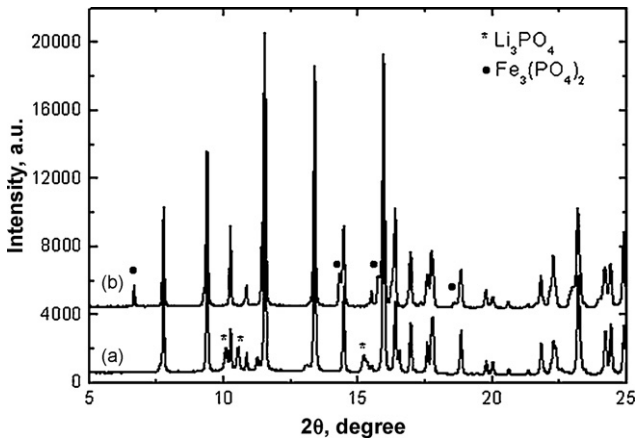

Fig. 3. High energy synchrotron XRD patterns of $LiFePO_4$ prepared via hydrothermal reaction: (a) with PVA and (b) at Li:P ratio of 2.5:1.

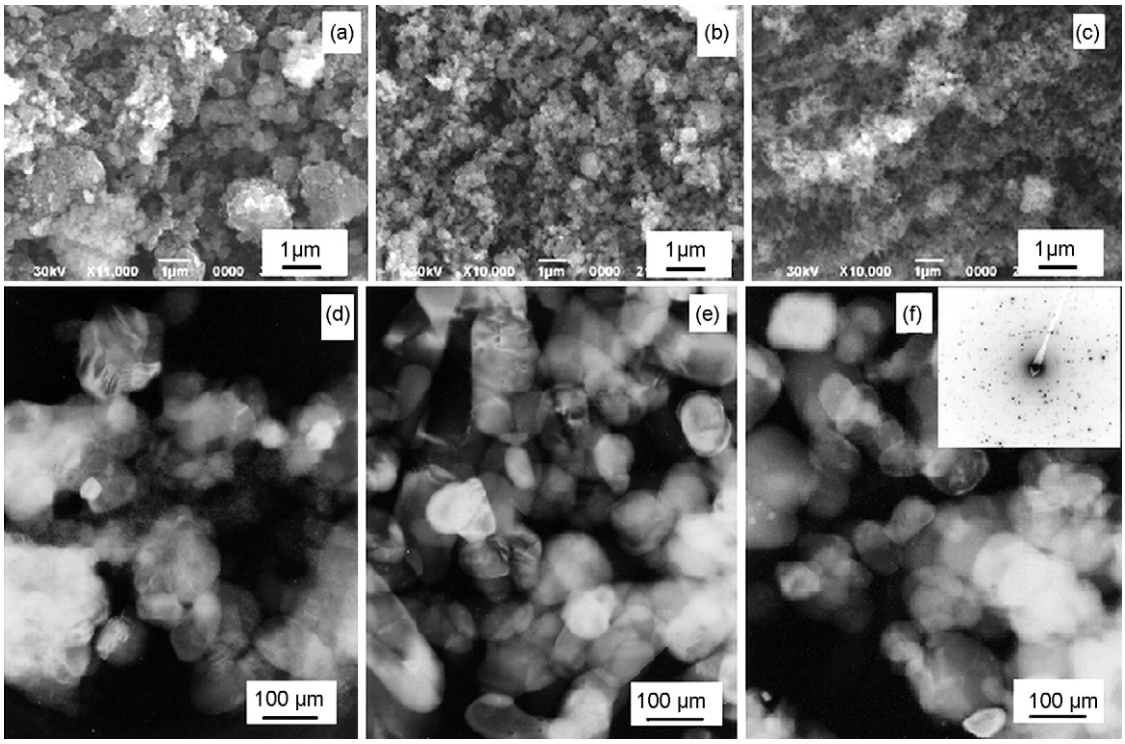

Fig. 4. SEM (a–c) and TEM (d–f) images of F-blank (a and d), F-citric (b and e), and F-ascorbic (c and f). Inset of (f) shows the corresponding electron diffraction.

acid-containing system. This product does not comprise Li_3PO_4 but monoclinic $Fe_3(PO_4)_2$ (JCPDS No. 39-0341) (Fig. 3b), which is consistent with the previous report by Kanamura and co-workers [21]. So it is reasonable to conclude that the impurity-free material is the result of the convergence of acidic effect and chelating effect from organic additive.

A further hydrothermal synthesis of $LiFePO_4$ was carried out at the same procedure with 0.83 mmol citric acid. The XRD data and corresponding Rietveld refinement reveal that the impurity Li_3PO_4 decreases to 0.33 wt.% (not shown). The failure to eliminate the impurity is just because the citric acid is not enough to help complete the conversion from Li_3PO_4 to $LiFePO_4$.

3.2. SEM and TEM

Fig. 4a–c shows the SEM images of as-prepared $LiFePO_4$ materials. It is clearly seen that the organic acids also regulate the particles. The F-blank sample comprises primary particles about 100 nm and some large agglomerates up to 1 μm, but the agglomerates are almost not visible in the mediated materials. Particularly, F-ascorbic consists of fine particles in a nearly mono-dispersive manner. The particle property was further characterized by TEM (Fig. 4d–f), and it is seen that the mediated sample is composed of nanocrystals which are uniformly dispersed with size about 50–100 nm (Fig. 4e and f), in violent contrast with the large agglomerates in F-blank (Fig. 4d). Electron diffraction (ED, inset of Fig. 4f) verifies the crystalline nature of these samples, in good agreement with XRD result.

It is believed that the difference in particle among these products is related to the adsorption of organic molecules or their decomposing derivatives on the crystal surface. These adsorbed molecules cover the surface of nanocrystals to prevent them from fusing together, leading to fine and dispersive particles [24,28]. Since the electrochemical behaviors of $LiFePO_4$, particularly the rate behavior, are largely determined by Li ion diffusion length within particle, the decrease of particle size definitely helps utilize the full capacity.

3.3. Charge and discharge performance

The electrochemical property was investigated by coin cell using Li foil as the count electrode. All the tests were implemented on three coin cells a batch, and the average results were adopted for the discussion. Fig. 5a shows their initial charge and discharge profiles. All the samples possess a flat plateau around 3.4 V, agreeing well with the two-phase ($LiFePO_4 \leftrightarrow FePO_4$) transformation model. A close look can discover slopes near the starting and end discharge, reminiscent of the existence of small single-phase domain as reported by Yamada and co-workers [29]. The F-blank shows a discharge capacities of 128 mAh g^{-1}, whereas the mediated samples show improved capacities, 153 mAh g^{-1} and 162 mAh g^{-1} for F-citric and F-ascorbic, respectively. Besides the high electrochemical activity, these mediated $LiFePO_4$ products also present enhanced cycle stability, as shown in Fig. 5b. For instance, F-ascorbic shows a stable cycling performance over 100 cycles at 0.2 C (34 mA g^{-1}), remaining 158 mAh g^{-1} at the 100th cycle comparing with the initial capacity of 160 mAh g^{-1}. By contrast, F-blank displays a gradual capacity fading over cycles, 101 mAh g^{-1} at the 100th cycle against an initial capacity of 121 mAh g^{-1}.

Fig. 6 compares the rate discharge capability of as-prepared three samples. As expected, the mediated $LiFePO_4$ samples display significantly enhanced performance over the blank $LiFePO_4$. In detail, F-blank discharges 128 mAh g^{-1} at 0.1 C, 97 mAh g^{-1} at 1 C, and 62 mAh g^{-1} at 5 C, whereas F-citric delivers 153 mAh g^{-1} at 0.1 C, 139 mAh g^{-1} at 1 C, and 95 mAh g^{-1} at 5 C. Moreover, F-ascorbic is able to deliver 162 mAh g^{-1}, 154 mAh g^{-1}, and 122 mAh g^{-1} at 0.1 C, 1 C, and 5 C, respectively. It is worth noting that the mediated $LiFePO_4$ also shows a stable discharge plateau upon increasing current, especially for F-ascorbic. Note that a parallel test was also carried out, and the very close results confirm the good reproducibility of the tests.

The improvement in electrochemical property can be rationally attributed to two key factors resulted from organic acid, i.e., impurity elimination and particle regulation. Since Li_3PO_4 may not

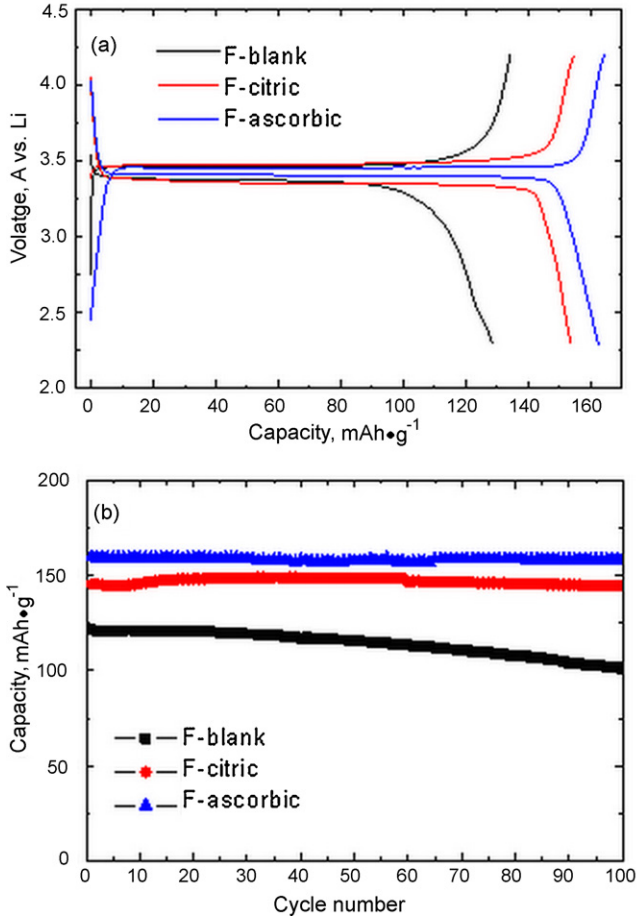

Fig. 5. (a) Initial charge and discharge curves at 0.1 C and (b) cycling performance at 0.2 C of $LiFePO_4$ samples of F-blank, F-citric, and F-ascorbic.

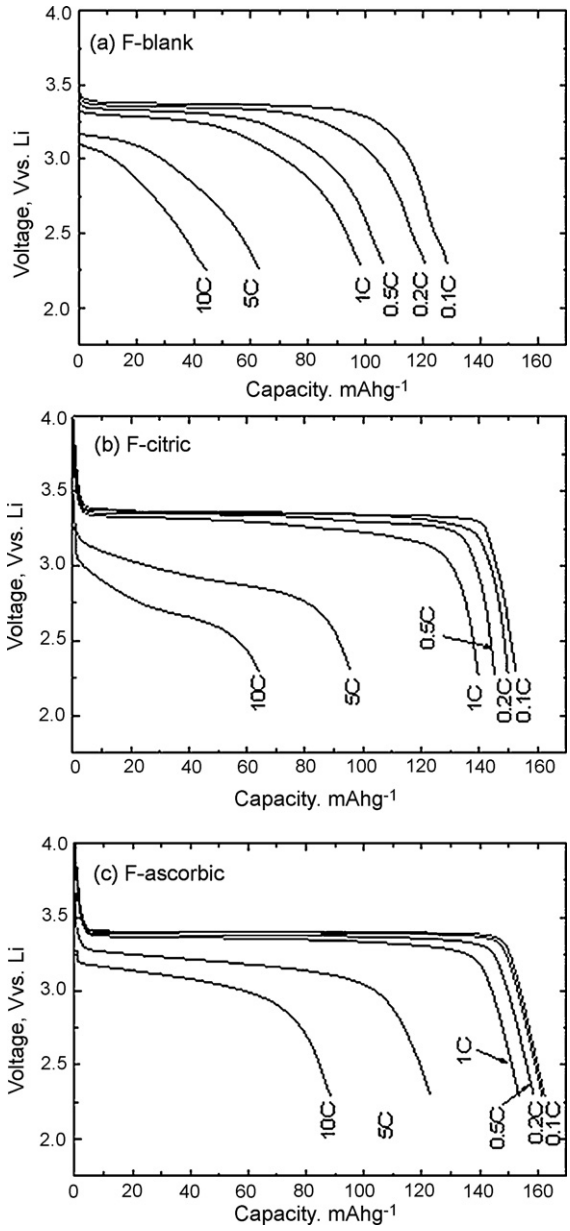

Fig. 6. Rate discharge capability of $LiFePO_4$ samples F-blank, F-citric, and F-ascorbic. The cells were first charged to 4.2 V at constant current of 0.1 C and then discharged to 2.3 V at a certain rate of current.

only destroy the integrity of conductivity, but also be detrimental to the electrode/electrolyte interphase [30], its elimination definitely improves the electrochemical behaviors. On the other hand, the regulation of particle decreases the length of Li ions diffusion in crystal, which enables fast kinetics of Li ions to achieve a high capacity and rate ability [16]. Another consideration from the homogeneity of nanocrystals is the alleviation of lattice strain upon Li insertion/extraction, which may cause particle cracking and capacity fading over cycling [31].

3.4. Raman spectroscopy

As for the difference of electrochemical behaviors between F-citric and F-ascorbic, it probably stems from the fact that ascorbic acid carbonizes upon hydrothermal process while citric acid does not. The carbon that is derived from ascorbic acid and loaded onto the surface of nanocrystal would be developed to a high conductive network in the following heating process. As a result, F-ascorbic will show a better conductive ability than F-citric despite of the fact that both are subjected to carbon-coating process later. To confirm this proposal, Raman spectroscopy was conducted on samples directly from hydrothermal reaction, and the spectra are presented in Fig. 7. A strong peak at 950 cm^{-1} accompanied with two other weak peaks at 995 cm^{-1} and 1069 cm^{-1} appears in all the spectra, which can be assigned to the stretching motion of PO_4^{3-} in $LiFePO_4$ [32], while peaks due to Fe_2O_3 or other Fe(III) impurity are absent [22]. Besides these peaks, the spectrum of F-ascorbic comprises a hump around 1400 cm^{-1} and a broad peak at 1575 cm^{-1}, indicative of the presence of carbon. The former can be assigned to the D mode originating from amorphous carbon, and the latter the G mode associated with the movement in opposite directions of two neighboring carbon atoms in a graphene sheet [4].

3.5. Electrochemical impedance spectroscopy

Electrochemical impedance spectroscopy was carried out to shed more light on the difference among these materials. The impedance was recorded on the coin batteries at different cycle stages, i.e. the fresh states and the state after 100 cycles. The corresponding Nyquist graphs of the spectra are presented in Fig. 8, and a simple equivalent circuit (inset of Fig. 8b) is established to simulate the spectra. The intercept at the Z_{real} axis in the high frequency refers to R_s, which includes electrolyte solution resistance and electric contacts resistance. The semi-circle in the high and middle frequency range is due to the charge transfer resistance (R_{ct}); and

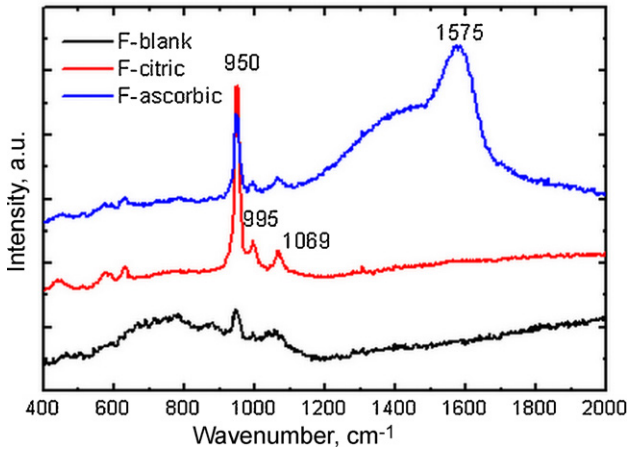

Fig. 7. Raman spectra of $LiFePO_4$ samples of F-blank, F-citric, and F-ascorbic before carbon coating.

the sloping line in the lower frequency represents lithium-ion diffusion resistance in electrode bulk, namely the Warburg impedance. It is found that the R_{ct} shows the trend F-ascorbic < F-citric < F-blank, either in the fresh state or cycled state. This suggests a higher charge transfer rate (mainly due to higher conductivity) for $LiFePO_4$ mediated by organic acid, consistent well with their electrochemical properties. Note that the R_{ct} of all three electrodes decrease after cycling, possibly due to gradual percolation of electrolyte or other activating effects, as discussed in the previous report [33].

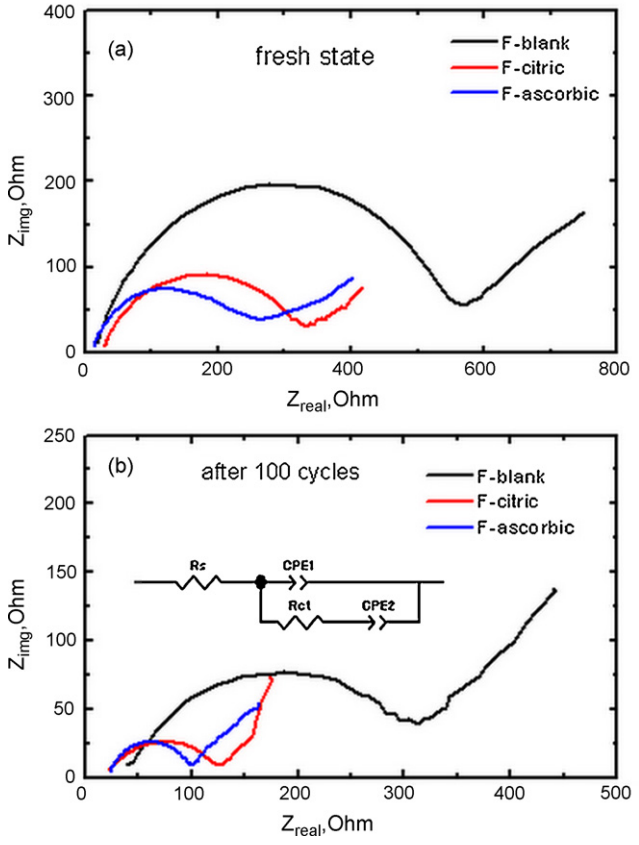

Fig. 8. Electrochemical impedance spectra of the electrodes containing different $LiFePO_4$ samples of F-blank, F-citric, and F-ascorbic under the fresh state (a) and after 100 cycles (b). Inset of (b) is the equivalent circuit established for the simulation of impedance spectra.

4. Conclusion

Well-crystallized $LiFePO_4$ nanoparticles were directly prepared via hydrothermal reaction operated at 230 °C for 30 min in the presence of organic acid. These mediated products show a single phase nature, as confirmed by high energy synchrotron radiation and corresponding structural analysis based on Rietveld refinement. SEM and TEM observations reveal that the $LiFePO_4$ mediated by organic acid consists of nearly homogenous nanocrystals with size of 50–100 nm, while the blank $LiFePO_4$ comprises some large agglomerates. Galvanostatic test shows that mediated $LiFePO_4$ exhibits a high electrochemical activity in terms of discharge capacity, cyclability, and rate capability. In particular, ascorbic acid-mediated $LiFePO_4$ can deliver 162 mAh g^{-1} at 0.1 C, 154 mAh g^{-1} at 1 C, and 122 mAh g^{-1} at 5 C. This adventure demonstrates the facile synthesis of high-performance $LiFePO_4$ via hydrothermal process in a short time, which is essentially feasible for other olivine materials. The attempt to decrease the operating temperature for making the hydrothermal synthesis not so critical is currently underway, which will further help expand its application in the preparation of electrode materials.

References

[1] A.K. Padhi, K.S. Nanjundaswamy, J.B. Goodenough, J. Electrochem. Soc. 144 (1997) 1188–1194.
[2] A.S. Andersson, J.O. Thomas, B. Kalska, L. Haggstrom, Electrochem. Solid State Lett. 3 (2000) 66–68.
[3] S.T. Myung, S. Komaba, N. Hirosaki, H. Yashiro, N. Kumagai, Electrochim. Acta 32 (2004) 4213–4222.
[4] K.F. Hsu, S.Y. Tsay, B.J. Hwang, J. Mater. Chem. 14 (2004) 2690–2695.
[5] A.V. Murugan, T. Muraliganth, A. Manthiram, J. Phys. Chem. C 112 (2008) 14665–14671.
[6] Y.G. Wang, Y.R. Wang, E. Hosono, K.X. Wang, H.S. Zhou, Angew. Chem. Int. Ed. 47 (2008) 1–6.
[7] S.Y. Chung, J.T. Bloking, Y.M. Chiang, Nat. Mater. 1 (2002) 123–128.
[8] M.S. Islam, D.J. Driscoll, C.A.J. Fisher, P.R. Slater, Chem. Mater. 17 (2005) 5085–5092.
[9] J.F. Ni, H.H. Zhou, J.T. Chen, X.X. Zhang, Mater. Lett. 59 (2005) 2361–2365.
[10] P.S. Herle, B. Ellis, N. Coombs, L.F. Nazar, Nat. Mater. 3 (2004) 147–152.
[11] H. Liu, Q. Cao, L.J. Fu, C. Li, Y.P. Wu, H.Q. Wu, Electrochem. Commun. 8 (2006) 1553–1557.
[12] S. Lim, C.S. Yoon, J. Cho, Chem. Mater. 20 (2008) 4560–4564.
[13] C.R. Sides, F. Croce, V.Y. Young, C.R. Martin, B. Scrosati, Electrochem. Solid-State Lett. 8 (2005) A484–A487.
[14] S. Franger, F.L. Cras, C. Bourbon, H. Rouault, J. Power Sources 119 (2003) 252–257.
[15] S.J. Kwon, C.W. Kim, W.T. Jeong, K.S. Lee, J. Power Sources 137 (2004) 93–99.
[16] C. Delacourt, P. Poizot, S. Levasseur, C. Masquelier, Electrochem. Solid-State Lett. 9 (2006) A325–A355.
[17] J. Yang, J.J. Xu, Electrochem. Solid-State Lett. 7 (2004) A515–A518.
[18] D.-H. Kim, J.k. Kim, Electrochem. Solid-State Lett. 9 (2006) A439–A442.
[19] S.F. Yang, P.Y. Zavalij, M.S. Whittingham, Electrochem. Commun. 3 (2001) 505–508.
[20] J. Chen, M.J. Vacchio, S. Wang, N. Chernova, P.Y. Zavalij, M.S. Whittingham, Solid State Ionics 178 (2008) 1676–1693.
[21] K. Dokko, K. Shiraishi, H. Nakano, K. Kanamura, J. Mater. Chem. 17 (2007) 4803–4810.
[22] K. Shiraishi, K. Dokko, K. Kanamura, J. Power Sources 146 (2005) 555–558.
[23] G. Meligrana, C. Gerbaldi, A. Tuel, S. Bodoardo, N. Penazzi, J. Power Sources 160 (2006) 516–522.
[24] B. Ellis, W.H. Kan, W.R.M. Makahnouk, L.F. Nazar, J. Mater. Chem. 17 (2007) 3248–3254.
[25] A. Kuwahara, S. Suzuki, M. Miyayama, Ceram. Int. 34 (2008) 863–866.
[26] F. Izumi, T. Ikeda, Mater. Sci. Forum (2000) 321–324.
[27] S. Zhou, H. Zhou, T. Miyoshi, M. Hibino, I. Honma, M. Ichihara, Adv. Mater. 16 (2004) 2012–2017.
[28] C. Lu, L. Qi, J. Yang, D. Zhang, N. Wu, J. Ma, J. Phys. Chem. B 108 (2004) 17825–17831.
[29] H. Koizumi, N. Sonoyama, R. Kanno, A. Yamada, Electrochem. Solid-State Lett. 8 (2005) A409–A413.
[30] D.Y.W. Yu, K. Donoue, T. Kadohata, T. Murata, S. Matsuta, S. Fujitani, J. Electrochem. Soc. 155 (2008) A526–A530.
[31] D. Wang, X. Wu, Z. Wang, L. Chen, J. Power Sources 140 (2005) 125–128.
[32] C.M. Burba, R. Frech, J. Electrochem. Soc. 151 (2004) A1032–A1038.
[33] J.F. Ni, H.H. Zhou, J.T. Chen, X.X. Zhang, Electrochim. Acta 53 (2008) 3075–3083.